Intelligent Reflecting Surfaces for Visible Light Positioning based on Received Power Measurements

Furkan Kokdogan and Sinan Gezici, *Senior Member, IEEE*

***Abstract*—In this paper, we formulate and analyze a received power based position estimation problem for visible light positioning (VLP) systems in presence of intelligent reflecting surfaces (IRSs). In the proposed problem formulation, a visible light communication (VLC) receiver collects signals from a number of light emitting diode (LED) transmitters via line-of-sight (LOS) paths and/or via reflections from IRSs. We derive the Cramér-Rao lower bound (CRLB) expression and the maximum likelihood (ML) estimator for generic three-dimensional positioning in the presence of IRSs with arbitrary configurations. In addition, we consider the problem of optimizing the orientations of IRSs when line-of-sight (LOS) paths are blocked, and propose an optimal adjustment approach for maximizing the received powers from IRSs based on analytic expressions, which can be solved in closed form or numerically. Since the optimal IRS orientations depend on the actual position of the VLC receiver, an N-step localization algorithm is proposed to perform adjustment of IRS orientations in the absence of any prior knowledge about the position of the VLC receiver. Performance of the proposed approach is evaluated via simulations and compared against the CRLB. It is deduced that although IRSs do no provide critical improvements in positioning accuracy in the presence of LOS signals from a sufficient number of LED transmitters, they can be very important in achieving accurate positioning when all or most of LOS paths are blocked.**

***Index Terms*– Intelligent reflecting surfaces, visible light positioning, estimation, Cramér-Rao lower bound, reconfigurable intelligent surfaces.**

I. Introduction

In the last decades, usage of light emitting diodes (LEDs) has been increasingly popular for illumination of indoor environments. Conventional light bulbs are slowly eradicating as the advantages of LEDs become more apparent in the contexts of illumination efficiency, longevity, environmental friendliness, and functionality [1]. LEDs consume considerably less power, have longer life time, do not contain toxic chemicals, and have dimming and color adjustment capabilities, which make them appealing to prefer over incandescent light bulbs. Besides these advantages, LEDs also have fast switching characteristics allowing data modulation schemes, which enables communication and positioning applications through the use of LEDs in indoor environments. In particular, the visible light positioning (VLP) concept has attracted significant attention from researchers. There are a number of studies in the literature proposing various position estimation algorithms and deriving theoretical limits on localization accuracy [2]–[5]. The received signal strength (RSS) information is commonly utilized in position estimation algorithms due to its low measurement cost and high accuracy in VLP systems [6]. Based on RSS measurements, closed form CRLB expressions are derived for position and orientation estimation in [7]. In [8], a simultaneous position and orientation (SPO) estimation algorithm is proposed by considering a mobile receiver equipped with multiple photo-detectors. Another SPO estimation approach is studied in [9] by using RSS measurements in a multi-input multi-output (MIMO) system.

Recently, emergence of configurable surfaces called intelligent reflecting surfaces (IRSs) has significant drawn attention in the area of radio frequency (RF) communications. IRSs consist of a number of low-cost passive elements that can control the phase, amplitude, frequency, and/or polarization of RF signals [10]. The authors in [10] present a detailed overview and historical perspective of the state of the art solutions for usage of IRSs in communication systems. In [11], an algorithm is proposed to minimize the total transmit power by means of jointly optimizing transmit and reflect beamforming via deployment of IRSs. In [12], it is shown that the use of IRS can help increase the energy efficiency of a wireless communication system by dynamically controlling the reflection coefficients of individual reflecting elements.

There also exist a number of studies that consider the usage of IRSs in visible light communication (VLC) systems [13]–[21]. Abdelhady et al. propose two types of IRSs for use in VLC systems; namely, metasurfaces and mirror arrays as the adaptation of IRS to the light propagation characteristics [13]. In addition, liquid crystal based IRSs are discussed in [14] and [21] for achieving signal coverage expansion and signal power enhancement in VLC systems. In [19], the use of IRSs is considered in a VLC system for replacing the traditional lens and steering the incident light beam, leading to wider field-of-view and intensity gain at the receiver. The authors of [15] develop a solution for joint optimization of time allocation, power control, and phase shift matrix under power constraints to maximize the energy efficiency in a downlink reconfigurable intelligent surface (RIS) aided VLC system. (The terms IRS and RIS are used interchangeably in the literature.) In [16], a low-complexity algorithm is proposed to maximize the achievable sum rate in a VLC system equipped with IRS. It is shown that IRS can help improve the rate performance and reduce blockage problems of VLC systems. In [17], the role of using IRS is to enhance the link reliability of a VLC system employing non-orthogonal multiple access (NOMA). It is deduced that IRS can significantly improve link reliability especially when the VLC channel is subject to blockage or random device orientation. In [18], the optimal orientation of IRS that maximizes the received power in a

Copyright (c) 2024 IEEE. Personal use of this material is permitted. However, permission to use this material for any other purposes must be obtained from the IEEE by sending a request to pubs-permissions@ieee.org.

F. Kokdogan and S. Gezici are with the Department of Electrical and Electronics Engineering, Bilkent University, Ankara 06800, Turkey, e-mails: {kokdogan,gezici}@ee.bilkent.edu.tr.

wireless communication system is analyzed. It is shown that the achievable rate can significantly be increased by adjusting the orientation of IRSs.

There are also a number of studies in the literature that investigate the use of IRSs in wireless positioning systems. In [22], it is shown that IRSs can be used to localize a user in the absence of a sufficient number of transmitters in a wireless network. The authors of [23] propose a device-to-device localization algorithm in an RF system of mmWave frequencies using RISs in the absence of access points. In [24], the use of RISs in a wireless localization system at mmWave frequencies is analyzed. The CRLB is derived and the reflect beamforming is optimized to improve positioning accuracy. In [25], a low complexity fingerprinting based localization algorithm is presented in a wireless communication system using RIS. The authors of [26] propose an angle-of-arrival (AoA) based positioning algorithm in an IRS-aided wireless communication system. In [27], the use of RIS is investigated for replacing the function of a remote cell in the downlink time-difference-of-arrival (DL-TDOA) measurement in 3GPP NR. It is shown that RIS-enabled localization along with a Kalman filter for tracking applications is a cost-effective solution with high accuracy. In [28], a distributed RIS assisted wireless positioning system is considered. A practical structure of indoor positioning is proposed consisting of two modes, namely, quasi-static and dynamic. The authors of [29] investigate the localization and orientation performance of synchronous and asynchronous signaling schemes by deriving the CRLB. In addition, a closed-form RIS phase profile that suits joint communication and localization is proposed. In [30], a general signal model of wideband systems with RISs is presented and the corresponding CRLB is derived to assess the localization performance of RIS-aided wideband systems.

Although there are a number of studies focusing on use of IRSs in both RF communication and VLC systems to improve performance and efficiency (and several other studies analyzing the use of IRSs in wireless positioning algorithms for RF systems), no studies have investigated the position estimation problem for IRS-aided VLP systems, which require different theoretical approaches compared to IRS-aided VLC systems [21]. In addition, as the light propagation and reflection characteristics are different from those of RF signals, specific analyses are required for VLP systems compared to wireless RF positioning systems. In this paper, we focus on a VLP system in which a VLC receiver equipped with a single photo-detector aims to estimate its position by utilizing the received power (equivalently, RSS) measurements from a number of LED transmitters by receiving signals from line-of-sight (LOS) paths and/or reflected paths via IRSs. The main contributions of this study to the existing literature can be summarized as follows:

- The problem of received power based position estimation for VLP systems in presence of IRSs is studied for the first time in the literature.
- A CRLB expression is derived for a generic three dimensional VLP system in the presence of IRSs with arbitrary configurations.
- A maximum likelihood (ML) estimator that utilizes the received power measurements from both LOS paths and reflected paths from IRSs is proposed for position estimation.
- The problem of optimizing the orientations of IRSs is considered when LOS paths are blocked, and an optimal adjustment approach is proposed for maximizing the received powers from IRSs based on analytic expressions, which can solved in closed form or numerically.
- An N-step localization algorithm is proposed to perform adjustment of IRS orientations (hence, to improve localization accuracy) in the absence of any prior knowledge about the position of the VLC receiver.

In addition, extensive simulations are conducted to investigate the effects of IRS parameters (such as reflection and directivity related parameters, and orientation vectors) and the blockage of LOS paths in various scenarios.

The rest of the paper is organized as follows. The system model is described in detail, and the CRLB expression and the ML estimator are derived in Section II. In Section III, the adjustment of IRS orientations is investigated analytically and solutions are derived to maximize the received power at the VLC receiver. Various simulations are conducted to inspect the performance of the proposed algorithms and to observe the effects of critical parameters in Section IV. Finally, concluding remarks are presented in Section VI.

II. VLP with Intelligent Reflecting Surfaces

We consider a VLP system with N_{L} LED transmitters at known locations denoted by $\boldsymbol{l}_1, \ldots, \boldsymbol{l}_{N_{\mathrm{L}}}$ and a VLC receiver at an unknown location represented by $\boldsymbol{x}$. The orientation vectors of the ith LED transmitter and the VLC receiver are assumed to be known and denoted by $\boldsymbol{n}_i$ and $\bar{\boldsymbol{n}}$, respectively, where $i \in \{1, \ldots, N_{\mathrm{L}}\}$.[1] In addition to the VLC receiver and the LED transmitters, there exist intelligent reflecting surfaces (IRSs) in the environment. In particular, there are N_{R} flat surfaces represented by $S_1, \ldots, S_{N_{\mathrm{R}}}$, which are at known locations $\tilde{\boldsymbol{l}}_1, \ldots, \tilde{\boldsymbol{l}}_{N_{\mathrm{R}}}$ and have known orientation vectors $\tilde{\boldsymbol{n}}_1, \ldots, \tilde{\boldsymbol{n}}_{N_{\mathrm{R}}}$. It is assumed that each flat surface causes glossy reflections [13], [32] and the surface reflectance coefficient is the same over each given surface; that is, ρ_k is used to represent the reflectance coefficient for the kth reflecting surface with $k \in \{1, \ldots, N_{\mathrm{R}}\}$.[2] Since the reflective surfaces are considered as a part of the system design, ρ_k and S_k (i.e., the surface equation) are assumed to be known for all $k \in \{1, \ldots, N_{\mathrm{R}}\}$. In this setup, the location $\tilde{\boldsymbol{l}}_k$ of the kth reflecting surface can correspond to any point on the surface (e.g., the center) as the surface equation is already known. The considered system model is illustrated in Fig. 1.[3]

The considered VLP system is asynchronous, meaning that the VLC receiver is not synchronized with the LED

[1] For example, $\bar{\boldsymbol{n}}$ can be measured via a gyroscope at the VLC receiver [31]. If the orientation of the VLC receiver is unknown, then joint position and orientation estimation should be performed for the VLC receiver, which is beyond the scope of our study.

[2] Glossy reflection [13, Section II.B] is defined as the combination of specular and diffuse components of reflection. Specular components are originated from perfectly smooth surfaces acting as mirrors while diffuse components are generated by scattering from rough surfaces.

[3] To keep the configuration of reflecting surfaces in the most generic form, we refer to each surface element as an IRS, which can have arbitrary location and orientation. In practice, a group of surface elements (i.e., "IRSs") are placed together to form a large reflecting surface, as shown in Fig. 2.

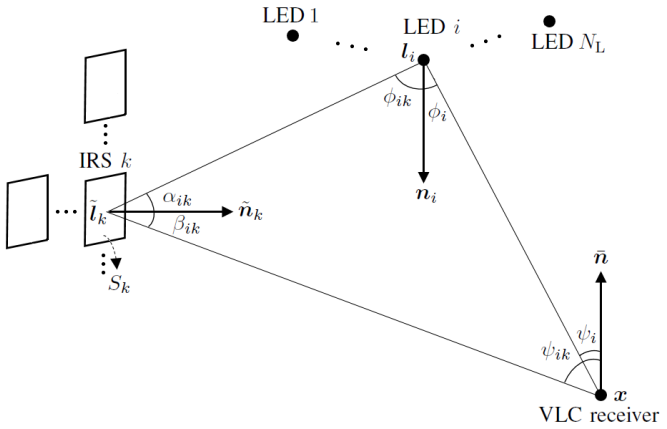

Fig. 1: A system with $N_{\rm L}$ LED transmitters, $N_{\rm R}$ intelligent reflecting surfaces (IRSs), and a VLC receiver is considered. In the figure, the parameters related to the ith LED transmitter and the kth IRS are shown. The orientation vectors are denoted by $\bar{\boldsymbol{n}}$, $\boldsymbol{n}_i$, and $\tilde{\boldsymbol{n}}_k$, and the locations are represented by $\boldsymbol{x}$, $\boldsymbol{l}_i$, and $\tilde{\boldsymbol{l}}_k$, all of which are *generic* three dimensional vectors. Also, the irradiance and incidence angles are named as in the figure.

transmitters [6]. In this system, the aim is to estimate the unknown location $\boldsymbol{x}$ of the VLC receiver based on power measurements at the VLC receiver due to the signals emitted by the LED transmitters. Considering a time division multiplexing approach, the VLC receiver can process signals coming from the LED transmitters separately [33], [34]. Then, considering a similar model to those in [35]–[37], the received power measurement at the VLC receiver due to the signal from the ith LED transmitter can be expressed as follows:[4]

$$P_{{\rm RX},i} = P_{{\rm TX},i}\, H_i^{\rm LOS}(\boldsymbol{x}) + P_{{\rm TX},i} \sum_{k=1}^{N_{\rm R}} \int_{S_k} dH_{i,k}^{\rm ref}\big(\boldsymbol{x}, \tilde{\boldsymbol{l}}_k\big) + \eta_i \tag{1}$$

for $i = 1, \ldots, N_{\rm L}$, where $P_{{\rm TX},i}$ is the transmit power of the ith LED transmitter, $H_i^{\rm LOS}(\boldsymbol{x})$ is the channel gain of the LOS path between the ith LED transmitter and the VLC receiver, $dH_{i,k}^{\rm ref}\big(\boldsymbol{x}, \tilde{\boldsymbol{l}}_k\big)$ is the channel gain of the path between the ith LED transmitter and the VLC receiver which makes a single reflection from an infinitesimally small area around $\tilde{\boldsymbol{l}}_k$ at the kth reflecting surface (please see Fig. 1), and η_i is a zero-mean Gaussian noise component with a variance of σ_i^2, which is independent of η_j for all $j \neq i$ [36].

As in [13], the field-of-view (FOV) of the photo-detector at the VLC receiver is assumed to 90^o by considering the use of a hemispherical lens at the VLC receiver [39]. Then, the channel gains in (1) can be calculated as [40][5]

$$H_i^{\rm LOS}(\boldsymbol{x}) = \frac{(m_i+1)A\left(\cos\phi_i\right)^{m_i} T_s(\psi_i) g(\psi_i) \cos\psi_i}{2\pi \|\boldsymbol{x} - \boldsymbol{l}_i\|^2} \tag{2}$$

[4]In practice, the incoming optical signal is converted to an electrical signal by the photo-detector at the VLC receiver. Then, the peak value of the correlation of the received electrical signal with delayed versions of the transmitted signal yields a measurement that is proportional to the received optical power [38]. Assuming that the responsivity of the photo-detector is known, the received power model in (1) can be obtained via scaling.

[5]As a practical scenario, the VLC receiver is assumed to be at a lower height than the IRSs and the LEDs. In the absence of this assumption, the formulas could be updated by eliminating the signals that would not be in the FOV of the VLC receiver.

and

$$dH_{i,k}^{\rm ref}\big(\boldsymbol{x}, \tilde{\boldsymbol{l}}_k\big) = (m_i+1)A(\cos\phi_{ik})^{m_i} \cos\alpha_{ik} R_k(\alpha_{ik}, \beta_{ik}) \frac{\cos\psi_{ik} T_s(\psi_{ik}) g(\psi_{ik})}{2\pi \|\boldsymbol{l}_i - \tilde{\boldsymbol{l}}_k\|^2 \|\boldsymbol{x} - \tilde{\boldsymbol{l}}_k\|^2}\, dS_k \tag{3}$$

with

$$R_k(\alpha_{ik}, \beta_{ik}) = \frac{\rho_k}{2\pi}\Big(2r_k \cos\beta_{ik} + (1-r_k)(\mu_k+1)(\cos(\beta_{ik} - \alpha_{ik}))^{\mu_k}\Big) \tag{4}$$

where m_i is the Lambertian order for the ith LED transmitter, A is the area of the photo-detector at the VLC receiver, ϕ_i and ψ_i are, respectively, the irradiance angle and the incidence angle for the LOS path between the ith LED transmitter and the VLC receiver, ϕ_{ik} and α_{ik} are, respectively, the irradiance angle and the incidence angle for the direct path between the ith LED transmitter and the reflective point $\tilde{\boldsymbol{l}}_k$ at the kth reflecting surface, β_{ik} and ψ_{ik} are, respectively, the irradiance angle and the incidence angle for the direct path between the reflective point $\tilde{\boldsymbol{l}}_k$ at the kth reflecting surface and the VLC receiver, dS_k represents an infinitesimally small area around $\tilde{\boldsymbol{l}}_k$ at the kth reflecting surface, and $T_s(\psi)$ and $g(\psi)$ are, respectively, the optical filter gain and the optical concentrator gain at the VLC receiver [35]. Commonly, $T_s(\psi)g(\psi)$ is designed to be constant [35]; hence, we set it to one in the remainder of the paper to simplify the notation. In (4), the first term represents the diffuse component and the second one is related to the specular component, with $r_k \in [0,1]$ specifying the fraction of diffuse component and μ_k determining the directivity of reflection [40]. (In the special case of $r_k = 1$, only diffuse reflection is considered and the model reduces to that in [35].)

The angles in (2) and (3) can be specified based on the following geometric relations (cf. Fig. 1): $(\boldsymbol{x} - \boldsymbol{l}_i)^T \boldsymbol{n}_i = \|\boldsymbol{x} - \boldsymbol{l}_i\| \cos\phi_i$, $(\boldsymbol{l}_i - \boldsymbol{x})^T \bar{\boldsymbol{n}} = \|\boldsymbol{l}_i - \boldsymbol{x}\| \cos\psi_i$, $(\tilde{\boldsymbol{l}}_k - \boldsymbol{l}_i)^T \boldsymbol{n}_i = \|\tilde{\boldsymbol{l}}_k - \boldsymbol{l}_i\| \cos\phi_{ik}$, $(\tilde{\boldsymbol{l}}_k - \boldsymbol{x})^T \bar{\boldsymbol{n}} = \|\tilde{\boldsymbol{l}}_k - \boldsymbol{x}\| \cos\psi_{ik}$, $(\boldsymbol{l}_i - \tilde{\boldsymbol{l}}_k)^T \tilde{\boldsymbol{n}}_k = \|\boldsymbol{l}_i - \tilde{\boldsymbol{l}}_k\| \cos\alpha_{ik}$, and $(\boldsymbol{x} - \tilde{\boldsymbol{l}}_k)^T \tilde{\boldsymbol{n}}_k = \|\boldsymbol{x} - \tilde{\boldsymbol{l}}_k\| \cos\beta_{ik}$. Then, (2) and (3) can be expressed via (4) as follows:

$$H_i^{\rm LOS}(\boldsymbol{x}) = \frac{(m_i+1)A\left((\boldsymbol{x} - \boldsymbol{l}_i)^T \boldsymbol{n}_i\right)^{m_i} (\boldsymbol{l}_i - \boldsymbol{x})^T \bar{\boldsymbol{n}}}{2\pi \|\boldsymbol{x} - \boldsymbol{l}_i\|^{m_i+3}} \tag{5}$$

$$dH_{i,k}^{\rm ref}\big(\boldsymbol{x}, \tilde{\boldsymbol{l}}_k\big) = \frac{(m_i+1)\left((\tilde{\boldsymbol{l}}_k - \boldsymbol{l}_i)^T \boldsymbol{n}_i\right)^{m_i} \left((\boldsymbol{l}_i - \tilde{\boldsymbol{l}}_k)^T \tilde{\boldsymbol{n}}_k\right)}{4\pi^2 \|\boldsymbol{l}_i - \tilde{\boldsymbol{l}}_k\|^{m_i+3} \|\boldsymbol{x} - \tilde{\boldsymbol{l}}_k\|^3}$$
$$A\,\rho_k \left((\tilde{\boldsymbol{l}}_k - \boldsymbol{x})^T \bar{\boldsymbol{n}}\right) dS_k \Bigg(2r_k \frac{\left((\boldsymbol{x} - \tilde{\boldsymbol{l}}_k)^T \tilde{\boldsymbol{n}}_k\right)}{\|\boldsymbol{x} - \tilde{\boldsymbol{l}}_k\|} + (1-r_k)(\mu_k+1)(\cos(\beta_{ik} - \alpha_{ik}))^{\mu_k}\Bigg). \tag{6}$$

In addition, $\cos(\beta_{ik} - \alpha_{ik})$ in (6) can be calculated as

$$\cos(\beta_{ik} - \alpha_{ik}) = \frac{\left((\boldsymbol{x} - \tilde{\boldsymbol{l}}_k)^T \tilde{\boldsymbol{n}}_k\right)\left((\boldsymbol{l}_i - \tilde{\boldsymbol{l}}_k)^T \tilde{\boldsymbol{n}}_k\right)}{\|\boldsymbol{x} - \tilde{\boldsymbol{l}}_k\| \|\boldsymbol{l}_i - \tilde{\boldsymbol{l}}_k\|} + \frac{\left\|(\boldsymbol{x} - \tilde{\boldsymbol{l}}_k) \times \tilde{\boldsymbol{n}}_k\right\| \left\|(\boldsymbol{l}_i - \tilde{\boldsymbol{l}}_k) \times \tilde{\boldsymbol{n}}_k\right\|}{\|\boldsymbol{x} - \tilde{\boldsymbol{l}}_k\| \|\boldsymbol{l}_i - \tilde{\boldsymbol{l}}_k\|} \tag{7}$$

where $\times$ denotes the cross product.

Remark 1: Only the direct paths among the LED transmitters, the IRSs, and the VLC receiver are considered in the preceding signal model. The main motivations behind omitting the other multipath components can be stated as follows: (i) In general, the received powers due to the direct paths are significantly higher than those due to the other multipath components. (Commonly, IRSs are made of highly reflecting materials for supporting visible light positioning [13]; hence, the direct paths from intelligent reflecting surfaces are expected to be stronger than the other multipath components, as well.) (ii) By omitting the multipath components, a tractable signal model is obtained, which facilitates theoretical analysis and intuitive explanations, leading to an understanding of the effects of IRSs for VLP systems, which have not been investigated previously for the setting considered in this paper. Hence, this study can be considered as an initial step for investigation of IRS-aided VLP systems. □

Remark 2: In this section, we employ a generic model for IRSs by considering the number, locations, areas, orientations, and reflectance coefficients of the surfaces as generic parameters. Hence, the derivations in this section are valid for different types of IRSs [13], [14], [21]. Similarly, LED transmitters and VLC receiver can have arbitrary locations and orientation vectors in the three-dimensional space. □

Since the noise components in (1) are independent zero-mean Gaussian random variables, the log-likelihood function for the unknown location $\boldsymbol{x}$ of the VLC receiver based on the received powers specified by (1) can be obtained as

$$\log p(\boldsymbol{P}_{\mathrm{RX}} \,|\, \boldsymbol{x}) = \tilde{k} - \sum_{i=1}^{N_{\mathrm{L}}} \frac{1}{2\sigma_i^2} \Bigg(P_{\mathrm{RX},i} - P_{\mathrm{TX},i}\, H_i^{\mathrm{LOS}}(\boldsymbol{x}) - P_{\mathrm{TX},i} \sum_{k=1}^{N_{\mathrm{R}}} \int_{S_k} dH_{i,k}^{\mathrm{ref}}\big(\boldsymbol{x}, \tilde{\boldsymbol{l}}_k\big) \Bigg)^2 \tag{8}$$

where $\boldsymbol{P}_{\mathrm{RX}} = [P_{\mathrm{RX},1} \cdots P_{\mathrm{RX},N_{\mathrm{L}}}]$ and $\tilde{k}$ is a constant independent of $\boldsymbol{x}$. Then, the ML estimator for the location of the VLC receiver, which is the maximizer of the log-likelihood function in (8), can be obtained as follows:

$$\widehat{\boldsymbol{x}}_{\mathrm{ML}} = \arg\min_{\boldsymbol{x}} \sum_{i=1}^{N_{\mathrm{L}}} \frac{1}{\sigma_i^2} \Bigg(P_{\mathrm{RX},i} - P_{\mathrm{TX},i}\, H_i^{\mathrm{LOS}}(\boldsymbol{x}) - P_{\mathrm{TX},i} \sum_{k=1}^{N_{\mathrm{R}}} \int_{S_k} dH_{i,k}^{\mathrm{ref}}\big(\boldsymbol{x}, \tilde{\boldsymbol{l}}_k\big) \Bigg)^2 \tag{9}$$

where H_i^{LOS} and $dH_{i,k}^{\mathrm{ref}}$ are evaluated based on the relations in (5)–(7).

To derive the CRLB, we first calculate the elements of the Fisher information matrix (FIM) [41], denoted by $\mathbf{I}(\boldsymbol{x})$, from (8), as follows:

$$[\mathbf{I}(\boldsymbol{x})]_{\ell_1,\ell_2} = \sum_{i=1}^{N_{\mathrm{L}}} \frac{(P_{\mathrm{TX},i})^2}{\sigma_i^2} \frac{\partial h_i(\boldsymbol{x})}{\partial x_{\ell_1}} \frac{\partial h_i(\boldsymbol{x})}{\partial x_{\ell_2}} \tag{10}$$

for $\ell_1, \ell_2 \in \{1,2,3\}$, where

$$h_i(\boldsymbol{x}) \triangleq H_i^{\mathrm{LOS}}(\boldsymbol{x}) + \sum_{k=1}^{N_{\mathrm{R}}} \int_{S_k} dH_{i,k}^{\mathrm{ref}}\big(\boldsymbol{x}, \tilde{\boldsymbol{l}}_k\big). \tag{11}$$

The partial derivatives of $h_i(\boldsymbol{x})$ in (11) can be stated as

$$\frac{\partial h_i(\boldsymbol{x})}{\partial x_\ell} = \frac{\partial H_i^{\mathrm{LOS}}(\boldsymbol{x})}{\partial x_\ell} + \sum_{k=1}^{N_{\mathrm{R}}} \int_{S_k} \frac{\partial dH_{i,k}^{\mathrm{ref}}\big(\boldsymbol{x}, \tilde{\boldsymbol{l}}_k\big)}{\partial x_\ell} \tag{12}$$

for $i \in \{1, \ldots, N_{\mathrm{L}}\}$ and $\ell \in \{1,2,3\}$. Via (12), we can observe the contributions of the LOS path and the reflected paths from the IRSs to the FIM in (10). Based on the expressions in (5)–(7), the partial derivatives in (12) can be calculated as

$$\begin{aligned}
\frac{\partial H_i^{\mathrm{LOS}}(\boldsymbol{x})}{\partial x_\ell} &= \frac{-(m_i+1)A}{2\pi \|\boldsymbol{x}-\boldsymbol{l}_i\|^{m_i+3}} \Bigg[\bar{n}_\ell \left((\boldsymbol{x}-\boldsymbol{l}_i)^T \boldsymbol{n}_i\right)^{m_i} \\
&- m_i n_{i,\ell} \left((\boldsymbol{x}-\boldsymbol{l}_i)^T \boldsymbol{n}_i\right)^{m_i-1} (\boldsymbol{l}_i - \boldsymbol{x})^T \bar{\boldsymbol{n}} \\
&+ \frac{(m_i+3)(x_\ell - l_{i,\ell}) \left((\boldsymbol{x}-\boldsymbol{l}_i)^T \boldsymbol{n}_i\right)^{m_i} (\boldsymbol{l}_i - \boldsymbol{x})^T \bar{\boldsymbol{n}}}{\|\boldsymbol{x}-\boldsymbol{l}_i\|^2} \Bigg],
\end{aligned} \tag{13}$$

$$\begin{aligned}
\frac{\partial dH_{i,k}^{\mathrm{ref}}(\boldsymbol{x}, \tilde{\boldsymbol{l}}_k)}{\partial x_\ell} &= \frac{(m_i+1)A \left((\tilde{\boldsymbol{l}}_k - \boldsymbol{l}_i)^T \boldsymbol{n}_i\right)^{m_i} (\boldsymbol{l}_i - \tilde{\boldsymbol{l}}_k)^T \tilde{\boldsymbol{n}}_k}{4\pi^2 \|\boldsymbol{l}_i - \tilde{\boldsymbol{l}}_k\|^{m_i+3}} \\
&\rho_k dS_k \Bigg\{ \Bigg[\left(\tilde{n}_{k,\ell} (\tilde{\boldsymbol{l}}_k - \boldsymbol{x})^T \bar{\boldsymbol{n}} - \bar{n}_\ell ((\boldsymbol{x} - \tilde{\boldsymbol{l}}_k)^T \tilde{\boldsymbol{n}}_k \right) \|\boldsymbol{x} - \tilde{\boldsymbol{l}}_k\|^{-4} \\
&- 4 \|\boldsymbol{x} - \tilde{\boldsymbol{l}}_k\|^{-6} (x_\ell - \tilde{l}_{k,\ell}) (\boldsymbol{x} - \tilde{\boldsymbol{l}}_k)^T \tilde{\boldsymbol{n}}_k (\tilde{\boldsymbol{l}}_k - \boldsymbol{x})^T \bar{\boldsymbol{n}} \Bigg] 2 r_k \\
&+ (1 - r_k)(\mu_k + 1) \Bigg[(\cos(\beta_{ik} - \alpha_{ik}))^{\mu_k} \big(- \bar{n}_\ell \|\boldsymbol{x} - \tilde{\boldsymbol{l}}_k\|^{-3} \\
&- 3 (\tilde{\boldsymbol{l}}_k - \boldsymbol{x})^T \bar{\boldsymbol{n}} \|\boldsymbol{x} - \tilde{\boldsymbol{l}}_k\|^{-5} (x_\ell - \tilde{l}_{k,\ell}) \big) \\
&+ \mu_k (\cos(\beta_{ik} - \alpha_{ik}))^{\mu_k - 1} \frac{(\tilde{\boldsymbol{l}}_k - \boldsymbol{x})^T \bar{\boldsymbol{n}}}{\|\boldsymbol{x} - \tilde{\boldsymbol{l}}_k\|^3} \frac{\partial \cos(\beta_{ik} - \alpha_{ik})}{\partial x_\ell} \Bigg] \Bigg\}
\end{aligned} \tag{14}$$

with

$$\begin{aligned}
\frac{\partial \cos(\beta_{ik} - \alpha_{ik})}{\partial x_\ell} &= \cos \alpha_{ik} \Big(\tilde{n}_{k,\ell} \|\boldsymbol{x} - \tilde{\boldsymbol{l}}_k\|^{-1} \\
&- (\boldsymbol{x} - \tilde{\boldsymbol{l}}_k)^T \tilde{\boldsymbol{n}}_k \|\boldsymbol{x} - \tilde{\boldsymbol{l}}_k\|^{-3} (x_\ell - \tilde{l}_{k,\ell}) \Big) + \\
&\sin \alpha_{ik} \Big(\big\| (\boldsymbol{x} - \tilde{\boldsymbol{l}}_k) \times \tilde{\boldsymbol{n}}_k \big\|^{-1} \big\{ \tilde{n}_{k,f(\ell+1)} \big[(x_\ell - \tilde{l}_{k,\ell}) \tilde{n}_{k,f(\ell+1)} \\
&- (x_{f(\ell+1)} - \tilde{l}_{k,f(\ell+1)}) \tilde{n}_{k,\ell} \big] - \\
&\tilde{n}_{k,f(\ell+2)} \big[(x_{f(\ell+2)} - \tilde{l}_{k,f(\ell+2)}) \tilde{n}_{k,\ell} - (x_\ell - \tilde{l}_{k,\ell}) \tilde{n}_{k,f(\ell+2)} \big] \big\} \\
&\|\boldsymbol{x} - \tilde{\boldsymbol{l}}_k\|^{-1} - \|\boldsymbol{x} - \tilde{\boldsymbol{l}}_k\|^{-3} (x_\ell - \tilde{l}_{k,l}) \big\| (\boldsymbol{x} - \tilde{\boldsymbol{l}}_k) \times \tilde{\boldsymbol{n}}_k \big\| \Big)
\end{aligned} \tag{15}$$

for $\ell \in \{1,2,3\}$, where $\bar{n}_\ell$, $n_{i,\ell}$, x_ℓ, $l_{i,\ell}$, $\tilde{n}_{k,\ell}$, and $\tilde{l}_{k,\ell}$ denote the ℓth components of vectors $\bar{\boldsymbol{n}}$, $\boldsymbol{n}_i$, $\boldsymbol{x}$, $\boldsymbol{l}_i$, $\tilde{\boldsymbol{n}}_k$, and $\tilde{\boldsymbol{l}}_k$, respectively, and $f(\ell)$ is defined as

$$f(\ell) = \begin{cases} \ell\,, & \text{if } \ell \leq 3 \\ \ell - 3\,, & \text{otherwise} \end{cases}. \tag{16}$$

As (13) is related to the LOS path between the ith LED transmitter and the VLC receiver, it is in the same form as [6, eq. (14)], where visible light positioning in the presence of LOS paths is investigated. However, the expressions in (14) and (15) are not available in the literature, which are associated with the additional position related information obtained via the IRSs.

Overall, the CRLB on the mean-squared error (MSE) of any unbiased position estimator $\widehat{\boldsymbol{x}}$ can be specified as $\mathrm{E}\{\|\widehat{\boldsymbol{x}} - \boldsymbol{x}\|^2\} \geq \mathrm{trace}\{\mathbf{I}(\boldsymbol{x})^{-1}\}$ based on the expressions in (7), (10), and (12)–(15). The derived CRLB expression is generic since no assumptions are made about the parameters of the IRSs such as their locations, orientations, and shapes. Also, it facilitates evaluation of position estimation accuracy in non-line-of-sight (NLOS) scenarios by setting the LOS components to zero. Moreover, via the proposed CRLB expression, desired parameters of IRSs can be optimized in order to enhance localization accuracy, as discussed next.

III. Adjustment of IRS Orientations

The locations of the IRSs, $\tilde{\boldsymbol{l}}_k$, are modeled as fixed parameters but it is assumed that their orientations $\tilde{\boldsymbol{n}}_k$ can be adjusted to improve the localization accuracy. For comparison purposes, a default configuration of IRS orientations can be defined such that all the IRSs are perpendicularly oriented to the wall they are located and they face towards the inside of the room. For example, in Fig. 2, $\tilde{\boldsymbol{n}}_k = [0\ 1\ 0]^T$ for the IRS located on the wall at $y = -2$ and $\tilde{\boldsymbol{n}}_k = [1\ 0\ 0]^T$ for the wall at $x = -2$. This configuration is referred to as "IRS-perpendicular" in the remainder of the paper. This configuration can be used when the position of the VLC receiver is completely unknown. However, when the position $\boldsymbol{x}$ of the VLC receiver is known even partially, i.e., when a position estimate $\hat{\boldsymbol{x}}$ exists, then the positioning accuracy can be improved by optimizing the orientations of the IRSs. Since the optimization of the CRLB derived in Section II with respect to the orientation vectors of all the IRSs would be impractically complex, we consider a fundamental approach that aims to increase the received power at the VLC receiver by adjusting the IRS orientations. Therefore, the objective is to find the orientation vectors, $\tilde{\boldsymbol{n}}_{ik}$, such that the $dH^{\mathrm{ref}}_{i,k}$ term in (3) is maximized for each LED. As stated before, the VLC receiver can extract the received signal from each LED individually via time division multiplexing. Hence, IRS orientations can be optimized for each LED separately.

The problem of maximizing the received power for the ith LED with respect to the IRS orientations can be expressed as follows:

$$\tilde{\boldsymbol{n}}^*_{ik} = \arg\max_{\tilde{\boldsymbol{n}}_k} \ dH^{\mathrm{ref}}_{i,k}\big(\tilde{\boldsymbol{n}}_k\big) \quad \text{s.t. } \|\tilde{\boldsymbol{n}}_k\| = 1 \tag{17}$$

for $k \in \{1, \ldots, N_{\mathrm{R}}\}$, where $dH^{\mathrm{ref}}_{i,k}$ in (3) is considered as a function of the IRS orientation $\tilde{\boldsymbol{n}}_k$, which can be stated as

$$dH^{\mathrm{ref}}_{i,k}\big(\tilde{\boldsymbol{n}}_k\big) = C \cos\alpha_{ik} R_k(\alpha_{ik}, \beta_{ik}) \tag{18}$$

with C representing the terms that do not depend on $\tilde{\boldsymbol{n}}_k$, namely,

$$C \triangleq (m_i+1)A(\cos\phi_{ik})^{m_i} \frac{\cos\psi_{ik} T_s(\psi_{ik}) g(\psi_{ik})}{2\pi \|\boldsymbol{l}_i - \tilde{\boldsymbol{l}}_k\|^2 \|\boldsymbol{x} - \tilde{\boldsymbol{l}}_k\|^2}\, dS_k. \tag{19}$$

It is noted that since the received power from each IRS is additive as shown in (1), the optimal IRS orientation can be found separately for each IRS for a given LED.

Substituting $R_k(\alpha_{ik}, \beta_{ik})$ in (4) into (18), we obtain

$$dH^{\mathrm{ref}}_{i,k}\big(\tilde{\boldsymbol{n}}_k\big) = C\frac{\rho_k}{2\pi}\cos\alpha_{ik}\Big(2r_k\cos\beta_{ik} + (1-r_k)(\mu_k+1)(\cos(\beta_{ik}-\alpha_{ik}))^{\mu_k}\Big). \tag{20}$$

Considering the system model in Fig. 1, it can be noted that the received power decreases when the vectors $(\boldsymbol{l}_i - \tilde{\boldsymbol{l}}_k)$, $(\boldsymbol{x} - \tilde{\boldsymbol{l}}_k)$ and $\tilde{\boldsymbol{n}}_k$ do not lie on the same plane. Therefore, the optimal $\tilde{\boldsymbol{n}}_k$ can be searched over the plane formed by $(\boldsymbol{l}_i - \tilde{\boldsymbol{l}}_k)$ and $(\boldsymbol{x} - \tilde{\boldsymbol{l}}_k)$. In this case, for fixed locations of the LED, the IRS, and the VLC receiver, the sum of α_{ik} and β_{ik} becomes constant, say θ_{ik}; that is, $\alpha_{ik} + \beta_{ik} \triangleq \theta_{ik}$. Accordingly, $dH^{\mathrm{ref}}_{i,k}$ in (20) can be stated as

$$dH^{\mathrm{ref}}_{i,k}\big(\tilde{\boldsymbol{n}}_k\big) = \bar{C}\cos\alpha_{ik}\Big(2r_k\cos(\theta_{ik}-\alpha_{ik}) + (1-r_k)(\mu_k+1)(\cos(\theta_{ik}-2\alpha_{ik}))^{\mu_k}\Big) \tag{21}$$

where $\bar{C} \triangleq C\rho_k/2\pi$. Based on (21), the solution of (17) can be derived for the cases of $r_k = 1$, $r_k = 0$, and $r_k \in (0,1)$ separately, as discussed below.

A. Solution for $r_k = 1$

When there is only diffuse reflection, i.e., when $r_k = 1$, $dH^{\mathrm{ref}}_{i,k}$ in (21) simplifies to

$$dH^{\mathrm{ref}}_{i,k}\big(\tilde{\boldsymbol{n}}_k\big) = 2\bar{C}\cos\alpha_{ik}\cos(\theta_{ik}-\alpha_{ik}). \tag{22}$$

The first-order derivative of $dH^{\mathrm{ref}}_{i,k}\big(\tilde{\boldsymbol{n}}_k\big)$ with respective to α_{ik} is given by

$$\frac{\partial dH^{\mathrm{ref}}_{i,k}\big(\tilde{\boldsymbol{n}}_k\big)}{\partial\alpha_{ik}} = 2\bar{C}\sin(\theta_{ik}-2\alpha_{ik}). \tag{23}$$

Setting the derivative in (23) to zero and considering that $\alpha_{ik} + \beta_{ik} = \theta_{ik}$, we obtain

$$\alpha_{ik} = \beta_{ik} = \frac{\theta_{ik}}{2}\,. \tag{24}$$

This solution is the maximizer as the second-order derivative can be shown to be negative at this point. This implies that, for the case of $r_k = 1$, the IRS orientation should be at the middle of the angle between the vectors $(\boldsymbol{l}_i - \tilde{\boldsymbol{l}}_k)$ and $(\boldsymbol{x} - \tilde{\boldsymbol{l}}_k)$ (please see Fig. 1).

B. Solution for $r_k = 0$

For $r_k = 0$, $dH^{\mathrm{ref}}_{i,k}$ in (21) can be simplified as

$$dH^{\mathrm{ref}}_{i,k}\big(\tilde{\boldsymbol{n}}_k\big) = \bar{C}(\mu_k+1)\cos\alpha_{ik}\cos(\theta_{ik}-2\alpha_{ik})^{\mu_k}. \tag{25}$$

Taking the first-order derivative with respective to α_{ik} yields

$$\frac{\partial dH^{\mathrm{ref}}_{i,k}\big(\tilde{\boldsymbol{n}}_k\big)}{\partial\alpha_{ik}} = \bar{C}(\mu_k+1)\Big(-\sin\alpha_{ik}\cos(\theta_{ik}-2\alpha_{ik})^{\mu_k} + 2\mu_k\cos\alpha_{ik}\sin(\theta_{ik}-2\alpha_{ik}\cos(\theta_{ik}-2\alpha_{ik})^{\mu_k-1})\Big). \tag{26}$$

Setting this derivative to zero results in the following condition:

$$\sin\alpha_{ik}\cos(\theta_{ik}-2\alpha_{ik}) = 2\mu_k\cos\alpha_{ik}\sin(\theta_{ik}-2\alpha_{ik}). \tag{27}$$

As a special case, if $\theta_{ik} = \frac{\pi}{2}$, i.e., if $(\boldsymbol{l}_i - \tilde{\boldsymbol{l}}_k) \perp (\boldsymbol{x} - \tilde{\boldsymbol{l}}_k)$, then (27) becomes

$$\sin\alpha_{ik}\sin(2\alpha_{ik}) = 2\mu_k\cos\alpha_{ik}\cos(2\alpha_{ik}) \tag{28}$$

which leads to the following relations:

$$\tan\alpha_{ik}\tan(2\alpha_{ik}) = 2\mu_k \tag{29}$$

$$\frac{2\tan^2\alpha_{ik}}{1-\tan^2\alpha_{ik}} = 2\mu_k \tag{30}$$

$$\alpha_{ik} = \tan^{-1}\left(\sqrt{\frac{\mu_k}{\mu_k+1}}\right) \tag{31}$$

It should be noted that there exist two α_{ik} values that satisfy (31). The positive value of α_{ik} must be chosen since the reflected light would be out of the FOV of the photo-detector at the VLC receiver for the negative value of α_{ik}.

If $\theta_{ik} \neq \frac{\pi}{2}$, then (27) becomes

$$\tan\alpha_{ik} = 2\mu_k\tan(\theta_{ik} - 2\alpha_{ik}). \tag{32}$$

After some manipulation, (32) results in the following equation:

$$\begin{aligned}&\tan^3\alpha_{ik} + (-2\mu_k\tan\theta_{ik} - 2\tan\theta_{ik})\tan^2\alpha_{ik}\\ &+ (-4\mu_k - 1)\tan\alpha_{ik} + 2\mu_k\tan\theta_{ik} = 0\end{aligned} \tag{33}$$

which is in the form of a cubic equation. The roots of this cubic equation can be obtained as follows:

$$\alpha_{ik,w} = \tan^{-1}\left(-\frac{1}{3a}\Big(b + \zeta^w D + \frac{\Delta_0}{\zeta^w D}\Big)\right) \tag{34}$$

for $w \in \{0,1,2\}$, where

$$\begin{aligned}a &= 1\\ b &= -2\mu_k\tan\theta_{ik} - 2\tan\theta_{ik}\\ c &= -4\mu_k - 1\\ d &= 2\mu_k\tan\theta_{ik}\\ \Delta_0 &= b^2 - 3ac\\ \Delta_1 &= 2b^3 - 9ac + 27a^2d\\ D &= \sqrt[3]{\frac{\Delta_1 + \sqrt{\Delta_1^2 - 4\Delta_0^3}}{2}}\\ \zeta &= \frac{-1+\sqrt{-3}}{2}\end{aligned} \tag{35}$$

Out of the three roots of the cubic equation given by (34) and (35), the root that satisfies $0 \leq \alpha_{ik,w} \leq \theta_{ik}$ must be chosen since the reflected light would be out of the FOV of the photo-detector at the VLC receiver otherwise.

Based on the preceding closed-form expressions, the optimal value of α_{ik} can be calculated, which also yields the optimal value of β_{ik} since $\alpha_{ik} + \beta_{ik} = \theta_{ik}$.

C. Solution for $r_k \in (0,1)$

For $r_k \in (0,1)$, the generic expression in (21) is used without any simplification, the first-order derivative of which is obtained as follows:

$$\begin{aligned}\frac{\partial dH_{i,k}^{\mathrm{ref}}(\tilde{\boldsymbol{n}}_k)}{\partial\alpha_{ik}} &= \bar{C}\Bigg(2r_k\Big(-\sin\alpha_{ik}\cos(\theta_{ik}-\alpha_{ik})\\ &+ \cos\alpha_{ik}\sin(\theta_{ik}-\alpha_{ik})\Big) + (1-r_k)(\mu_k+1)\Big(-\sin\alpha_{ik}\\ &\cos(\theta_{ik}-2\alpha_{ik})^{\mu_k} + 2\mu_k\cos\alpha_{ik}\cos(\theta_{ik}-2\alpha_{ik})^{\mu_k-1}\Big)\Bigg).\end{aligned} \tag{36}$$

Setting this derivative to zero yields the following equation:

$$\begin{aligned}&\frac{2r_k\sin(\theta_{ik}-2\alpha_{ik})}{(1-r_k)(\mu_k+1)} + \cos(\theta_{ik}-2\alpha_{ik})^{\mu_k-1}\big(-\sin\alpha_{ik}\\ &\cos(\theta_{ik}-2\alpha_{ik}) + 2\mu_k\cos\alpha_{ik}\sin(\theta_{ik}-2\alpha_{ik})\big) = 0\end{aligned} \tag{37}$$

From (37), α_{ik} cannot be expressed in closed form. However, it can be numerically solved to find the optimal values of α_{ik} and β_{ik} rapidly, e.g., the bisection method can be applied.

For all the cases in Sections III-A, III-B, and III-C, $\tilde{\boldsymbol{n}}_k$ can be expressed based on the obtained values of α_{ik} and β_{ik}. Let $\boldsymbol{u}_{ik} \triangleq \frac{(\boldsymbol{l}_i - \tilde{\boldsymbol{l}}_k)}{\|\boldsymbol{l}_i - \tilde{\boldsymbol{l}}_k\|}$ and $\boldsymbol{v}_{ik} \triangleq \frac{(\boldsymbol{x} - \tilde{\boldsymbol{l}}_k)}{\|\boldsymbol{x} - \tilde{\boldsymbol{l}}_k\|}$. By geometry, we have (see Fig. 1)

$$\begin{aligned}\boldsymbol{u}_{ik}^T\tilde{\boldsymbol{n}}_k &= \cos\alpha_{ik}\\ \boldsymbol{v}_{ik}^T\tilde{\boldsymbol{n}}_k &= \cos\beta_{ik}\end{aligned} \tag{38}$$

It is noted that $\tilde{\boldsymbol{n}}_k$ can be expressed as a linear combination of $\boldsymbol{u}_{ik}$ and $\boldsymbol{v}_{ik}$ since all these vectors lie on the same plane. Letting $\tilde{\boldsymbol{n}}_k \triangleq p\boldsymbol{u}_{ik} + q\boldsymbol{v}_{ik}$ and substituting this into (38), we obtain

$$\begin{aligned}\boldsymbol{u}_{ik}^T(p\boldsymbol{u}_{ik} + q\boldsymbol{v}_{ik}) &= \cos\alpha_{ik}\\ \boldsymbol{v}_{ik}^T(p\boldsymbol{u}_{ik} + q\boldsymbol{v}_{ik}) &= \cos\beta_{ik}\end{aligned} \tag{39}$$

By noting that $\|\boldsymbol{u}_{ik}\| = \|\boldsymbol{v}_{ik}\| = 1$, (39) leads to the following relations:

$$\begin{aligned}p + q\boldsymbol{u}_{ik}^T\boldsymbol{v}_{ik} &= \cos\alpha_{ik}\\ p\boldsymbol{u}_{ik}^T\boldsymbol{v}_{ik} + q &= \cos\beta_{ik}\end{aligned} \tag{40}$$

Solving this system of equations for p and q yields

$$\begin{aligned}p &= \frac{\cos\alpha_{ik} - \boldsymbol{u}_{ik}^T\boldsymbol{v}_{ik}\cos\beta_{ik}}{1-(\boldsymbol{u}_{ik}^T\boldsymbol{v}_{ik})^2}\\ q &= \frac{\boldsymbol{u}_{ik}^T\boldsymbol{v}_{ik}\cos\alpha_{ik} - \cos\beta_{ik}}{(\boldsymbol{u}_{ik}^T\boldsymbol{v}_{ik})^2 - 1}\end{aligned} \tag{41}$$

Hence, the orientation vector $\tilde{\boldsymbol{n}}_k$ that maximizes $dH_{i,k}^{\mathrm{ref}}$ can be expressed, based on the obtained values of α_{ik} and β_{ik} in Sections III-A, III-B, and III-C, as follows:

$$\begin{aligned}\tilde{\boldsymbol{n}}_{ik}^* &= \frac{\cos\alpha_{ik} - \boldsymbol{u}_{ik}^T\boldsymbol{v}_{ik}\cos\beta_{ik}}{1-(\boldsymbol{u}_{ik}^T\boldsymbol{v}_{ik})^2}\boldsymbol{u}_{ik}\\ &+ \frac{\boldsymbol{u}_{ik}^T\boldsymbol{v}_{ik}\cos\alpha_{ik} - \cos\beta_{ik}}{(\boldsymbol{u}_{ik}^T\boldsymbol{v}_{ik})^2 - 1}\boldsymbol{v}_{ik}\end{aligned} \tag{42}$$

for $k \in \{1,\ldots,N_{\mathrm{R}}\}$ and $i \in \{1,\ldots,N_{\mathrm{L}}\}$.

D. N-Step Localization Algorithm

For calculating the optimal orientation vectors obtained in Section III, the position of the VLC receiver should be known. At the beginning of the localization process and when there exists no prior information about the position of the VLC receiver, optimal IRS orientations cannot be calculated. In that case, we start with the "IRS-perpendicular" configuration (described at the beginning of Section III), and perform position estimation based on this configuration. Then, using the resulting position estimate, the IRS orientations can be optimized and the resulting configuration is called "IRS-focused", which can lead to more accurate localization. This procedure can be repeated a number of times to improve adjustment of IRS orientations and consequently, the positioning accuracy. Algorithm 1 below, which is called "N-Step Localization Algorithm", defines a procedure to improve the positioning accuracy with multiple usage of "IRS-focused" configurations.

It should be emphasized that in tracking applications, the position estimate of the VLC receiver at the previous time step can be used as a rough position estimate to determine IRS orientations.[6] In such cases, it may not be necessary to start the N-step localization algorithm with the "IRS-perpendicular" configuration. Also, the frequency of adjusting IRS orientations can be determined based on the mobility of the VLC receiver.

Algorithm 1 N-Step Localization Algorithm

1: Estimate position of VLC receiver as $\hat{\boldsymbol{x}}$ using "IRS-perpendicular" configuration
2: **for** $i = 1 \rightarrow \mathrm{N} - 1$ **do**
3: Based on $\hat{\boldsymbol{x}}$, calculate $\tilde{\boldsymbol{n}}_{ik}^{*}$ as in Section III to obtain "IRS-focused" configuration
4: Estimate position of VLC receiver as $\hat{\boldsymbol{x}}$ using "IRS-focused" configuration
5: **end for**

Remark 3: As discussed in Section IV, the received signals from the IRSs become crucial for localization when the LOS paths between the LEDs and the VLC receiver are blocked. Therefore, optimization of IRS orientations is important for NLOS scenarios. On the other hand, when LOS paths exist between the LEDs and the VLC receiver, it is not critical to adjust the orientation vectors of the IRSs. □

Remark 4: In wireless RF systems, IRSs (RISs) are composed of an array of passive scattering elements based on meta-materials, each of which can independently apply desired phase shifts on incoming RF signals. On the other hand, in visible light systems, IRSs are commonly made of an array of mirrors or an array of optical metasurface reflectors (patches) [13], [14], [21]. In this paper, we consider IRSs as intelligent mirror arrays, where the orientation vectors of IRSs can be adjusted. (Actually, the analysis and derivations in Section II also work for any type of IRSs since we keep all the parameters of IRSs generic.) Therefore, during the optimization of the IRSs, we focus on the adjustment of IRS orientations, which is completely different from the IRS design in wireless RF systems, where phase shifts imposed by IRSs are optimized. □

Remark 5: The N-step localization algorithm (Algorithm 1) involves calculating the IRS orientations that maximize the received power at the VLC receiver and estimating the position of the VLC receiver position via (9). It is noted that solving (9) requires a search over a three-dimensional space whereas the calculation the IRS orientations is simply performed via closed form expressions for $r_k = 0$ and $r_k = 1$ or a one-dimensional search for $r_k \in (0, 1)$. Therefore, the complexity of the N-step localization algorithm can be argued to be about N times the complexity of ML estimation for the position of the VLC receiver. □

IV. Simulation Results

In this section, simulations are conducted to evaluate the performance of the proposed positioning approach for VLP in the presence of IRSs. A room with dimensions $4 \times 4 \times 3$ meters (width, depth and height, respectively) is considered. The number of LED transmitters is taken as $N_{\mathrm{L}} = 4$ and they are placed at the following locations: $\{(-1, 1, 3), (1, 1, 3), (1, -1, 3), (-1, -1, 3)\}$ (all in meters) such that the room is covered symmetrically, where $(0, 0, 0)$ corresponds to the center of the room floor. The orientation vectors, $\boldsymbol{n}_i$'s, are taken as $[0, 0, -1]^T$ $\forall i$ meaning that all the LEDs face downwards. The transmit powers of the LEDs, $P_{\mathrm{TX},i}$, are set to $5\,\mathrm{W}$, and m_i's are taken as 1 $\forall i$. Also, the orientation of the receiver is specified as $\bar{\boldsymbol{n}} = [0, 0, 1]^T$, i.e., it faces upwards. Moreover, the noise variances are assumed to be the same, that is, $\sigma_i^2 = \sigma^2$ for $i = 1, \ldots, N_{\mathrm{L}}$. On each wall, $N_{\mathrm{R}}/4$ IRSs are used, which are placed as a $\sqrt{N_{\mathrm{R}}/4} \times \sqrt{N_{\mathrm{R}}/4}$ array. N_{R} is taken as 1764 in the simulations; hence, there are 21×21 IRSs on each wall, as shown in Fig. 2. The width and the height of each rectangular IRS is set to $w_u = 4$ cm and $h_u = 2$ cm, respectively. Thus, the area of each IRS, S_k, is set to $8\ \mathrm{cm}^2$ $\forall k$. The IRSs are separated from each other with $w_d = 2$ cm horizontally and $h_d = 1$ cm vertically to prevent the inter-element blockage as shown in detail in Fig. 3. IRSs are located to cover the center of the wall both horizontally and vertically for each wall, meaning that the center of the two-dimensional IRS array coincides with the center point of the wall. As the default configuration, the normal vector of each IRS is chosen such that the IRSs are perpendicular to the wall. Finally, the reflectance coefficient of the IRS elements is set to $\rho_k = 0.95$ $\forall k$. A visualization of the overall configuration of the simulation environment can be seen in Fig. 2.

The fraction of diffuse component r_k, the directivity of reflection μ_k, and the orientation of IRS $\tilde{\boldsymbol{n}}_k$ are significant parameters that affect the positioning accuracy. To investigate the effects of these parameters on the positioning accuracy, three sets of (r_k, μ_k) pair are chosen as $\{(1, -), (0.5, 5), (0, 5)\}$.[7] Also, the orientation vectors of the IRSs are designed for two different configurations. The first configuration is "IRS-perpendicular" in which all the IRSs are oriented as perpendicular to the wall and face inside. The second configuration is "IRS-focused" in which the orientations of the IRSs are

[6] If the knowledge of a mobility model exists for the VLC receiver, a tracking filter, such extended Kalman filter, can be integrated with the proposed position estimation approach.

[7] When the value of r_k is 1, the received power is independent of the value of μ_k (see (4)). Therefore this pair is stated as $(r_k, \mu_k) = (1, -)$.

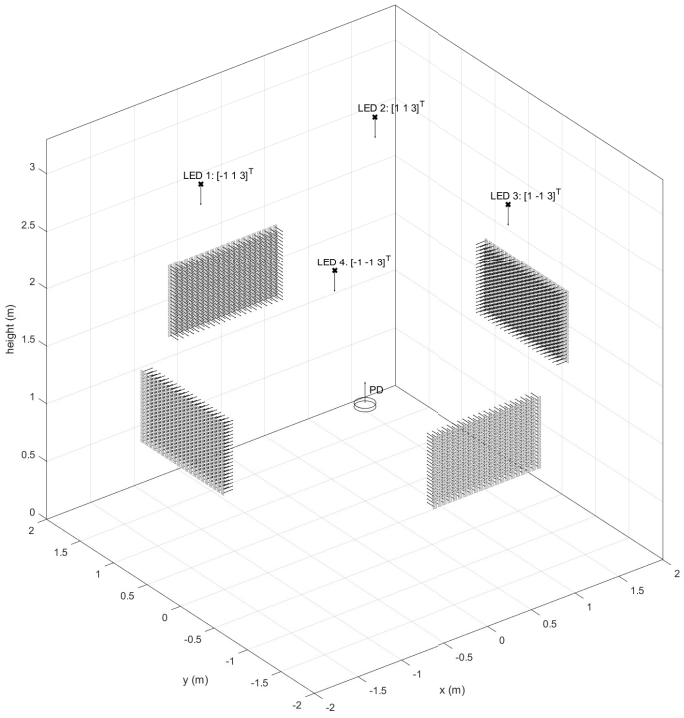

Fig. 2: Visualization of the room setup used in the simulations. Gray rectangles on the walls represent IRSs and small black arrows represent their normal vectors.

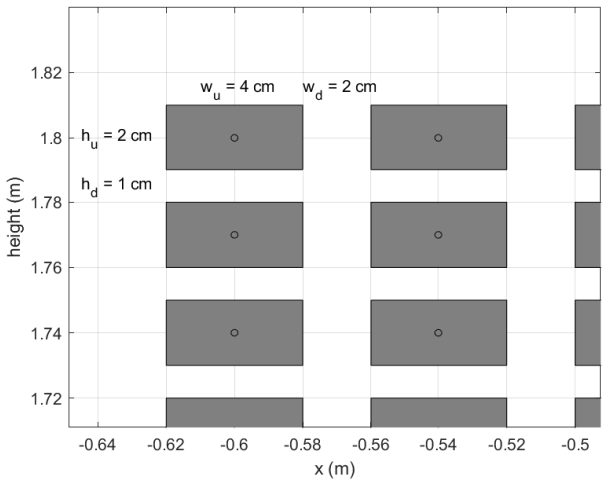

Fig. 3: A zoomed view of configuration of IRSs on the wall at $y = -2$.

optimized as in Section III to maximize the received power at the VLC receiver. The actual position of the VLC receiver is used when optimizing the orientation vectors to provide a benchmark. (When the position of the VLC receiver is unknown, the IRS orientations will be adjusted during the implementation of the N-step localization algorithm.) As an example, we illustrate in Fig. 4 the optimal orientations of the IRSs to maximize the received power at the VLC receiver from each LED transmitter. (The top view of the room is displayed for ease of interpretation.) In the simulations, the receiver unit is located at $(0.5, 0.5, 0.85)$ meters and the CRLB derived in Section II is calculated as a benchmark for three dimensional

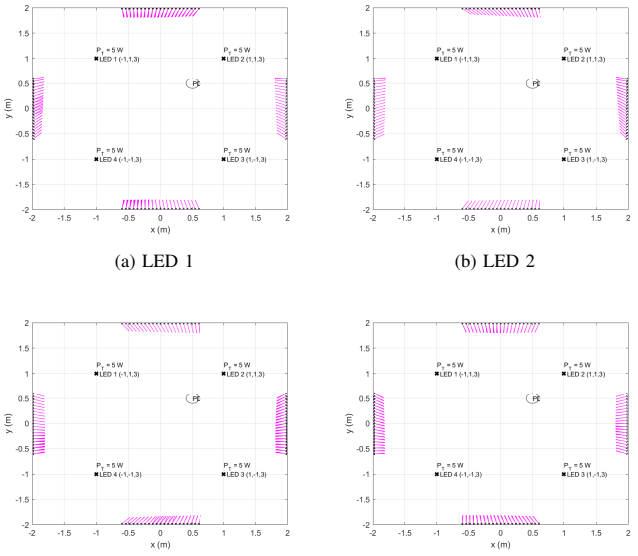

(a) LED 1 (b) LED 2

(c) LED 3 (d) LED 4

Fig. 4: Top view of the room illustrating the optimized orientations of IRSs for each LED.

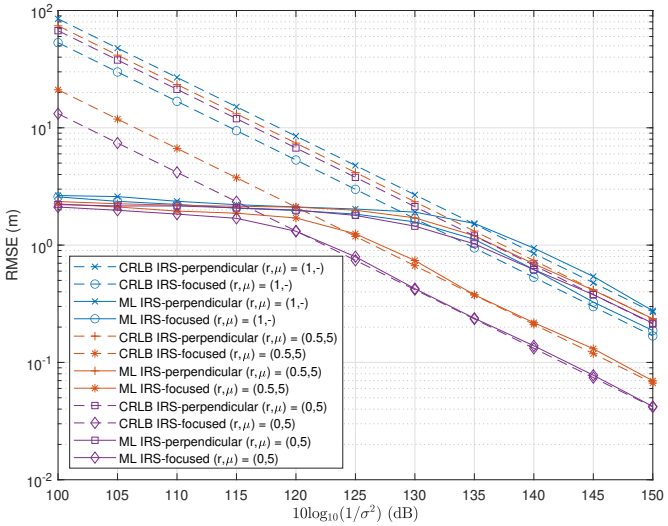

Fig. 5: RMSE versus $10\log_{10}(1/\sigma^2)$ for various settings in NLOS scenario.

localization accuracy with different values of the noise variance σ^2. It is assumed that the LOS path is not available and the VLC receiver only utilizes the reflections from the IRSs for position estimation. The ML estimator defined in (9) is used to estimate the position of the VLC receiver. For each noise variance value, the simulation is repeated for 1000 times and the root mean squared error (RMSE) is calculated. The simulations are repeated for each (r_k, μ_k) pair for both IRS-perpendicular and IRS-focused configurations to see the effects of these parameters on the positioning accuracy.

In Fig. 5, the RMSEs of the ML estimators and the CRLBs are plotted versus the noise variance for different parameter sets and IRS configurations.[8] It is observed that the RMSE

[8]The range of σ^2 values in the figure is compatible with the practical values reported in the literature [37] considering that varying the noise variance would have similar effects to changing the transmit powers of the LEDs.

of the ML estimator for the IRS-perpendicular configuration with $r_k = 1$ achieves an accuracy of 27.5 cm for the lowest noise variance (i.e., the highest signal-to-noise ratio (SNR)) in the figure.[9] For the parameter set $(r_k, \mu_k) = (0.5, 5)$, the RMSE reduces to 23.5 cm, whereas for $(r_k, \mu_k) = (0, 5)$, the RMSE becomes 21.5 cm. Thus, it can be argued that when the LOS paths are not available, increasing the directivity of the reflected paths, i.e., μ_k, improves the positioning accuracy. For the IRS-focused configuration, it is seen from Fig. 5 that adjusting the orientations of the IRSs such that the received power at the VLC receiver is maximized improves the positioning accuracy significantly. When the IRSs are focused to the location of the VLC receiver, the RMSEs of the ML estimators reduce to 16.8 cm, 6.6 cm, and 4.2 cm for the parameter sets $(r_k, \mu_k) = (1, -)$, $(r_k, \mu_k) = (0.5, 5)$, and $(r_k, \mu_k) = (0, 5)$, respectively. This means that the performance of the IRS-perpendicular configuration can be achieved with 5 dB, 10 dB and 15 dB lower SNR by using the IRS-focused configurations, respectively for these (r_k, μ_k) pairs. It should be noted that the resulting accuracy improvement is asymptotic since the perfect knowledge of the receiver location is assumed in these scenarios. Thus, this constitutes a lower bound on the achievable RMSE when optimizing the IRS orientations. The achievability of this bound in practical situations is illustrated next.

To investigate the performance of the N-step localization algorithm, simulations are conducted with $\mathrm{N} = \{2, 3\}$, which are repeated for each (r_k, μ_k) pair considered in the previous scenario. In this case, the VLC receiver is assumed to have an unknown position initially, and the IRS-perpendicular configuration is used in the first step. Then, the IRS orientations are focused in the next step(s) as described in Algorithm 1. It can be seen from Fig. 6 that for $10\log_{10}(1/\sigma^2) = 125$ dB, 2-Step and 3-Step localization algorithms improve the positioning accuracy significantly compared to the IRS-perpendicular configuration but cannot achieve the CRLB, which is obtained based on the perfect knowledge of the receiver position. For $10\log_{10}(1/\sigma^2) = 130$ dB, the 3-step localization algorithm gets very close to the CRLB. For lower noise variance, both the 2-step and 3-step localization algorithms converge to the CRLB. Therefore, the positioning accuracy can be significantly improved for $(r_k, \mu_k) = (0, 5)$ even though the VLC receiver has an unknown position initially. From Fig. 7, which is obtained for $(r_k, \mu_k) = (0.5, 5)$, it is observed that the positioning accuracy improvement is reduced but still both algorithms converge to the CRLB, which assumes the perfect knowledge of the receiver position for optimizing IRS orientations, when $10\log_{10}(1/\sigma^2)$ is higher than 140 dB. In addition, Fig. 8 suggests that the improvement in accuracy is limited for $(r_k, \mu_k) = (1, -)$ and a lower value of σ^2 is needed for convergence to the CRLB. This means that when the IRSs perform only diffuse reflection, IRS focusing becomes less effective.

[9]It is noticed that for large values of noise variances (low SNR values), the RMSEs of the estimators for all configurations are below the CRLBs. This is due to the fact that the possible locations of the VLC receiver in the room are limited to $4 \times 4 \times 3$ meters in three dimensions, and the ML estimators perform the search over this space. On the other hand, the CRLB derivations do not assume any prior information about the location of the VLC receiver; hence, can lead to larger values than RMSEs in very noisy cases.

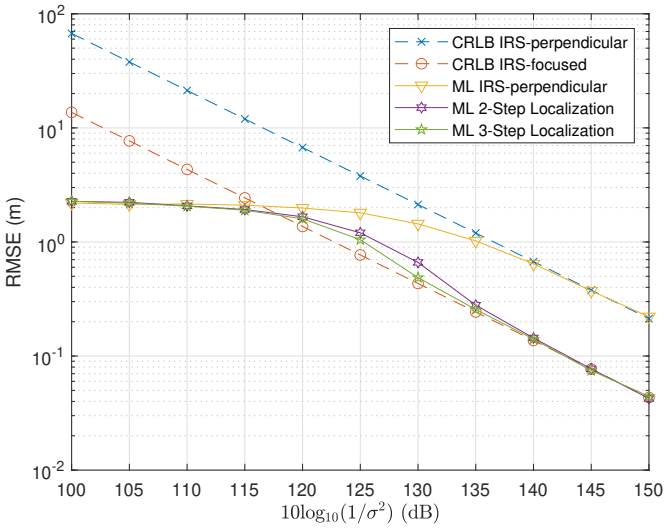

Fig. 6: RMSE versus $10\log_{10}(1/\sigma^2)$ for $(r_k, \mu_k) = (0, 5)$.

For investigating the convergence of the N-step localization algorithm, we conduct simulations for various values of N, namely, $\mathrm{N} \in \{0, 1, \ldots, 8\}$ by setting (r_k, μ_k) to $(0, 5)$. It should be noted that $\mathrm{N} = 0$ means that only the "IRS-perpendicular" configuration is used to estimate the position of the VLC receiver, which is also referred to as "ML IRS-perpendicular" in the paper. To observe the convergence behaviour of the proposed algorithm for different noise variances, we set $10\log_{10}(1/\sigma^2)$ to four different values, which are 125 dB, 130 dB, 135 dB, and 140 dB. From Fig. 9, it can be seen that the RMSE of the N-step localization algorithm converges to "CRLB IRS-focused" and to the RMSE of "ML IRS-focused" for values of $10\log_{10}(1/\sigma^2)$ above 125 dB while it gets very close to "CRLB IRS-focused" at 125 dB. It can be observed that only 1 step is sufficient for convergence at high SNRs such as 140 dB whereas it takes 3 steps at SNR of 130 dB. Overall, numerical results illustrate that the performance of the N-step localization algorithm rapidly converges to "CRLB IRS-focused" at sufficiently high SNRs. Convergence at high SNRs can be justified by the asymptotic unbiasedness and efficiency properties of the ML estimator [41].

In addition to the preceding simulations conducted for NLOS environments, we also consider scenarios in which the received powers from LOS and IRS paths are utilized together. We calculate the CRLBs for those scenarios to investigate the effects of the received power from the IRS elements when a subset of LOS components is present. The first scenario is that the VLC receiver gets signals from only the LOS paths between itself and all the LEDs, i.e., the IRSs are not present. This scenario is referred to as "4 LOS + 0 IRS". In the second scenario, the VLC receiver obtains power measurements from both the LOS and IRS paths for all the LEDs (referred to as "4 LOS + 4 IRS"). In the third scenario, it is assumed that the LOS path from one of the randomly chosen LED is unavailable, hence, the VLC receiver utilizes only the LOS signals from the remaining LEDs while the IRS elements are not present (referred to as "3 LOS + 0 IRS"). In the fourth scenario, on top of the LOS signals from these three

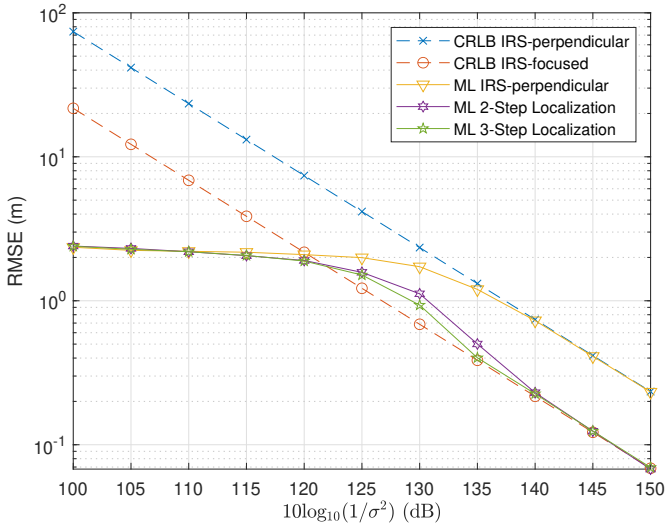

Fig. 7: RMSE versus $10\log_{10}(1/\sigma^2)$ for $(r_k, \mu_k) = (0.5, 5)$.

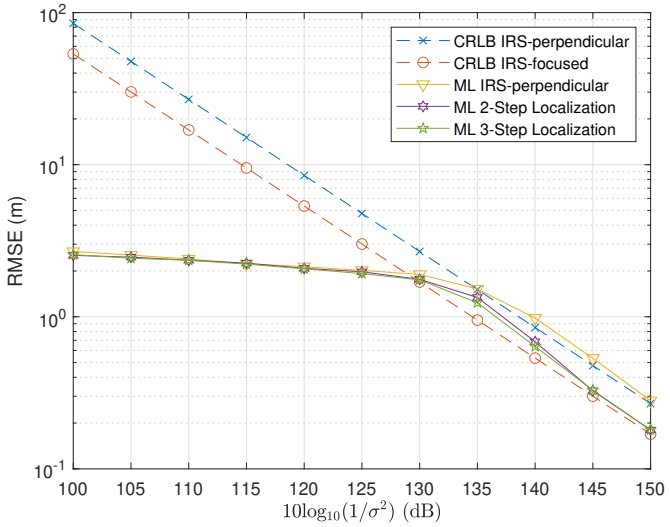

Fig. 8: RMSE versus $10\log_{10}(1/\sigma^2)$ for $(r_k, \mu_k) = (1, -)$.

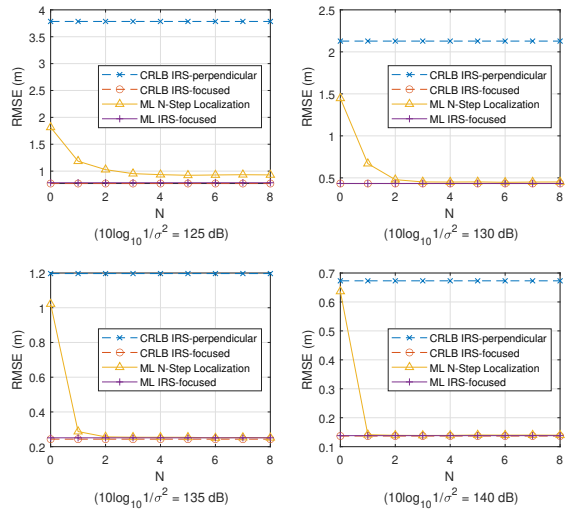

Fig. 9: RMSEs of ML estimator with IRS-focused configuration and of N-step localization algorithm versus N considering various noise levels, together with the CRLBs.

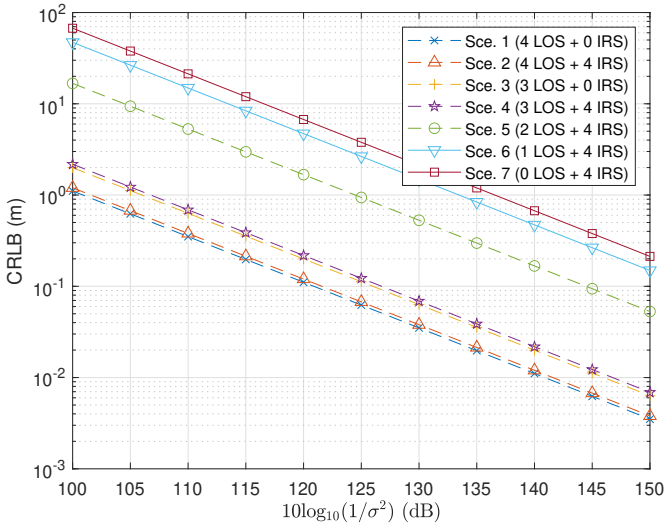

Fig. 10: CRLB versus $10\log_{10}(1/\sigma^2)$ for various IRS-aided scenarios when the VLC receiver is placed at $\boldsymbol{x} = [0.5\ 0.5\ 0.85]^T$ meters.

LEDs (as specified in the third scenario), there also exist IRSs which reflect the signals from all the LEDs (referred to as "3 LOS + 4 IRS"). In other words, only the LOS path of one randomly chosen LED is not present in this scenario. As the fifth scenario, the LOS paths from two randomly chosen LEDs are assumed to be unavailable; however, all of the reflected paths are present from the IRSs for all the LEDs (referred to as "2 LOS + 4 IRS"). In the sixth scenario, only one LOS path from a randomly chosen LED is available and all the IRS reflections are present (referred to as "1 LOS + 4 IRS"). In the seventh and final scenario, no LOS paths are available and the positioning is performed based only on the components from the IRSs (referred to as "0 LOS + 4 IRS"). For the scenarios involving a blockage of LOS path(s) from a subset of LEDs, the CRLB is calculated and averaged out based on 1000 random selections of LEDs to remove the effects of the choice of blocked LEDs. In addition, the IRS-perpendicular configuration is used in all of the scenarios described above involving the use of IRSs.

Fig. 10 illustrates the CRLBs for the seven scenarios described in the previous paragraph. From the figure, it is seen that the scenario with "0 LOS + 4 IRS" (Scenario 7) has the lowest performance (highest CRLB), as expected. When an LOS LED is present (Scenario 6), the accuracy improves slightly. The scenario with "2 LOS + 4 IRS" has notable improvement in accuracy compared to Scenarios 6 and 7. In addition, the scenarios with 3 and 4 LOS LEDs significantly outperform the remaining three scenarios since information from 3 or 4 LOS signals can provide accurate position information. As expected, the case with 4 LOS LEDs has the best performance. It is also observed that using the powers obtained via IRSs does not improve the positioning accuracy when 3 or 4 LOS LEDs are present; on the contrary, the positioning accuracy is slightly decreased. The reason for this interesting situation is that an increase in total received power does not always result in improved localization performance. This is

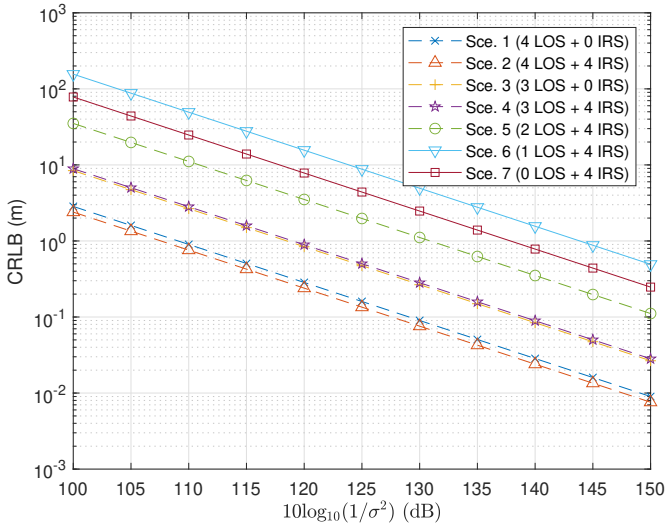

Fig. 11: CRLB versus $10\log_{10}(1/\sigma^2)$ for various IRS-aided scenarios when the VLC receiver is placed at $\boldsymbol{x} = [1.5\ 1.5\ 0.85]^T$ meters.

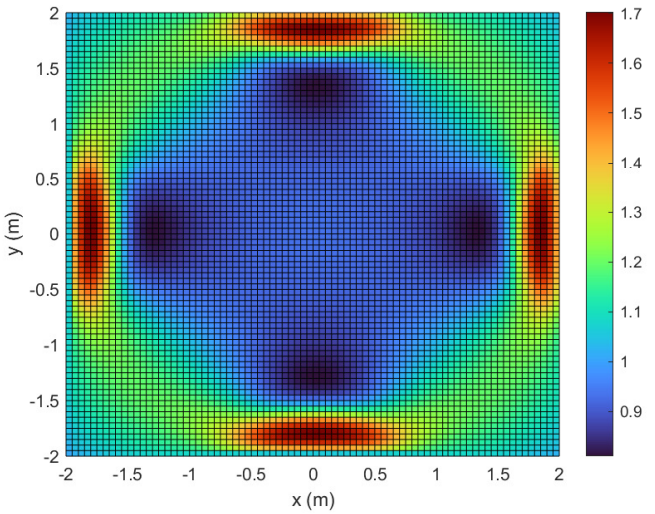

Fig. 12: Ratio between the CRLB using only LOS components and the CRLB using both LOS and IRS components.

because the partial derivatives with respect to the components of the unknown position vector $\boldsymbol{x}$ can have opposite signs for LOS and IRS paths depending on the position of the VLC receiver (please see (10) and (12)). To observe this, the receiver is moved to another location, namely, $(1.5, 1.5, 0.85)$ meters and the CRLB calculations are repeated, as depicted in Fig. 11. It is noted that the scenario with "4 LOS + 4 IRS" has the best performance in this case. For this position of the VLC receiver, the partial derivatives in (12) have the same sign, hence, the CRLB decreases. Using the reflected signals from the IRSs slightly increases the positioning performance in this case. (The improvement is slight since the LOS paths are significantly stronger.) As another remark, it is observed that the scenario with "0 LOS + 4 IRS" outperforms the scenario with "1 LOS + 4 IRS". This is due to the fact that the presence of a LOS component from a single LED affects the positioning accuracy negatively for the given position of the VLC receiver.[10]

We also perform additional simulations to have a better understanding of effects of utilizing the IRSs on positioning accuracy in the presence of LOS paths for all the LEDs. For this purpose, the VLC receiver is moved across the room horizontally by fixing its height to 0.85 meter and the corresponding CRLB values are calculated for the three-dimensional localization problem. Since the aim is to investigate the contribution of reflected signals from the IRSs on the positioning accuracy, the VLC receiver is assumed to get LOS signals from all the LEDs. At each position of the VLC receiver, the CRLB is first obtained without the presence of IRS paths. Then, the CRLB calculation is repeated using the IRS-perpendicular configuration and utilizing both the LOS and IRS components. In order to have a clear interpretation, the ratio of the CRLB values, namely, the CRLB based only on the LOS paths divided by the CRLB based on both the LOS and IRS paths, is plotted in Fig. 12. It can be seen that the contribution of the IRSs to the positioning accuracy becomes significant when the VLC receiver is away from the center of the room especially when it is close to the center of a wall. Conversely, when the VLC receiver is closer to the room center, the contribution of the IRSs to the accuracy is very small or even slightly negative in some areas.

Overall, it is concluded that when LOS signals are available at the VLC receiver from a sufficiently high number of LED transmitters, utilization of signals from IRSs may not provide significant improvements in position estimation based on received power measurements and can even degrade localization accuracy in some cases (see Figs. .10 and 12). However, IRSs facilitate position estimation even in the absence of LOS signals from the LED transmitters or even when most of the LOS paths between the LED transmitters and the VLC receiver are blocked (Figs. 10 and 11). Therefore, IRSs are useful for VLP systems based on received power measurements particularly for NLOS environments. As illustrated in Figs. 5–8, the proposed adjustment technique for IRS orientations can also be employed to provide significant enhancements to localization accuracy of VLP systems in NLOS scenarios.

V. Alternative Approach for Adjustment of IRS Orientations

In Section III, it is assumed that the VLC receiver can gather information from LEDs at different time intervals, i.e., time division multiplexing is employed. This facilitates the optimal adjustment of IRS orientations for each LED; hence, it is possible to maximize the received power at the VLC receiver due to the reflected path from the kth IRS unit for each LED separately. However, this requires the adjustment of IRS orientations N_{L} times to perform a position estimation, which can introduce latency to the system. To avoid this delay, an alternative approach is to consider the use of frequency (or, code) division multiplexing so that the LEDs can transmit signals at the same time, and the IRS orientations are adjusted

[10]For the scenarios in Fig. 10 and Fig. 11 that involve the use of IRSs, the IRS-perpendicular configuration is used for a clear and simple explanation of the effects of IRSs. If focused IRSs are employed instead of perpendicular IRSs, improved accuracy levels can be achieved.

to maximize the sum of the received powers of all the signals emitted from the LEDs and reflected from the kth IRS unit. This optimization problem can be formulated as follows:

$$\tilde{\boldsymbol{n}}_k^* = \arg\max_{\tilde{\boldsymbol{n}}_k} \sum_{i=1}^{N_{\mathrm{L}}} dH_{i,k}^{\mathrm{ref}}\left(\tilde{\boldsymbol{n}}_k\right) \quad \text{s.t. } \|\tilde{\boldsymbol{n}}_k\| = 1 \tag{43}$$

where $dH_{i,k}^{\mathrm{ref}}$ is as defined for (17) and $\tilde{\boldsymbol{n}}_k$ refers to the orientation vector for the kth IRS unit. It is noted that unlike the approach in Section III, only one orientation is determined for each IRS unit.

As an approach to solve this optimization problem, the optimal orientation vectors $\tilde{\boldsymbol{n}}_k^*$ can be regarded as rotated versions of the orientation vectors in the IRS-perpendicular configuration. For example, the IRS units at wall $x = -2$ in Fig. 2 have the orientation vector $\tilde{\boldsymbol{n}}_k = [1\ 0\ 0]^{\mathrm{T}}\ \forall k$. All the possible orientations that face inside the room can be obtained via rotating this vector around the y and z axes. Likewise, for the IRS units located on the wall at $y = -2$, the orientation vector $\tilde{\boldsymbol{n}}_k = [0\ 1\ 0]^{\mathrm{T}}\ \forall k$ can be rotated around the x and z axes to obtain an arbitrary orientation facing inside the room. Thus, the optimal orientation vector $\tilde{\boldsymbol{n}}_k^*$ can be expressed as follows:

$$\tilde{\boldsymbol{n}}_k^* = \boldsymbol{R}(\omega_{x,k}, \omega_{y,k}, \omega_{z,k})\tilde{\boldsymbol{n}}_k \tag{44}$$

where $\boldsymbol{R}(\omega_{x,k}, \omega_{y,k}, \omega_{z,k})$ is the three-dimensional rotation matrix and $\omega_{x,k}$, $\omega_{y,k}$ and $\omega_{z,k}$ are the angles of rotation around the x, y and z axes, respectively, for the kth IRS unit, which can be expressed as

$$\boldsymbol{R}(\omega_{x,k}, \omega_{y,k}, \omega_{z,k}) = \boldsymbol{R}(\omega_{x,k})\boldsymbol{R}(\omega_{y,k})\boldsymbol{R}(\omega_{z,k}) \tag{45}$$

with

$$\boldsymbol{R}(\omega_{x,k}) = \begin{bmatrix} 1 & 0 & 0 \\ 0 & \cos\omega_{x,k} & -\sin\omega_{x,k} \\ 0 & \sin\omega_{x,k} & \cos\omega_{x,k} \end{bmatrix} \tag{46}$$

$$\boldsymbol{R}(\omega_{y,k}) = \begin{bmatrix} \cos\omega_{y,k} & 0 & \sin\omega_{y,k} \\ 0 & 1 & 0 \\ -\sin\omega_{y,k} & 0 & \cos\omega_{y,k} \end{bmatrix} \tag{47}$$

$$\boldsymbol{R}(\omega_{z,k}) = \begin{bmatrix} \cos\omega_{z,k} & -\sin\omega_{z,k} & 0 \\ \sin\omega_{z,k} & \cos\omega_{z,k} & 0 \\ 0 & 0 & 1 \end{bmatrix}. \tag{48}$$

Rotation around the x axis is not needed for the IRS units located on the walls at $x = -2$ and $x = 2$, i.e., $\omega_{x,k} = 0$. In this case, the problem reduces to finding the angles $\omega_{y,k}$ and $\omega_{z,k}$ for kth IRS unit as follows:

$$(\omega_{y,k}^*, \omega_{z,k}^*) = \arg\max_{\omega_{y,k},\omega_{z,k}} \sum_{i=1}^{N_L} dH_{i,k}^{\mathrm{ref}}\left(\boldsymbol{R}(0, \omega_{y,k}, \omega_{z,k})\tilde{\boldsymbol{n}}_k\right) \tag{49}$$

where $\tilde{\boldsymbol{n}}_k = [1\ 0\ 0]^{\mathrm{T}}\ \forall k$ for the wall at $x = -2$ and $\tilde{\boldsymbol{n}}_k = [-1\ 0\ 0]^{\mathrm{T}}\ \forall k$ for the wall at $x = 2$. Likewise, the rotation around the y axis is not needed for the IRS units located on the walls at $y = -2$ and $y = 2$, i.e., $\omega_{y,k} = 0$. In this case, the problem reduces to finding the angles $\omega_{x,k}$ and $\omega_{z,k}$ as

$$(\omega_{x,k}^*, \omega_{z,k}^*) = \arg\max_{\omega_{x,k},\omega_{z,k}} \sum_{i=1}^{N_L} dH_{i,k}^{\mathrm{ref}}\left(\boldsymbol{R}(\omega_{x,k}, 0, \omega_{z,k})\tilde{\boldsymbol{n}}_k\right) \tag{50}$$

where $\tilde{\boldsymbol{n}}_k = [0\ 1\ 0]^{\mathrm{T}}\ \forall k$ for the wall at $y = -2$ and $\tilde{\boldsymbol{n}}_k = [0\ -1\ 0]^{\mathrm{T}}\ \forall k$ for the wall at $y = 2$. Based on the formulations in (49) and (50), the optimal adjustments of IRS units can be found by using numerical optimization methods.

Simulations are conducted to evaluate the performance of this alternative IRS adjustment approach. The optimal orientation vectors are obtained via particle swarm optimization (PSO) using the actual position of the VLC receiver and the resulting IRS configuration is referred to as "IRS-avg.focused". The value of the (r_k, μ_k) pair is taken as $(0, 5)$. From Fig. 13, it is observed that the performance of the IRS-avg.focused configuration is significantly better than the IRS-perpendicular configuration yet slightly worse than the IRS-focused configuration, which optimizes the IRS orientations for each LED separately. Since the IRS-avg.focused configuration employs a single optimized IRS configuration for all the LEDs instead of optimizing the orientations for each LED separately, it has the advantages of achieving a lower latency and facilitating easier implementation without requiring time division multiplexing, in addition to improving the positioning accuracy compared to the IRS-perpendicular configuration. This approach can also be useful in tracking applications in which the VLC receiver moves rapidly in a given environment.

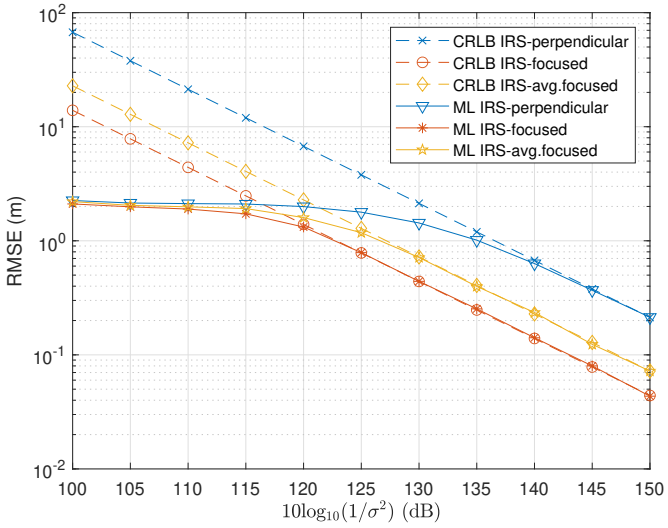

Fig. 13: RMSE versus $10\log_{10}(1/\sigma^2)$ for different IRS configurations in NLOS scenario, where the IRS-focused configuration requires time division multiplexing for adjusting IRS orientations separately for each LED.

VI. Concluding Remarks

In this paper, we have formulated the received power based position estimation problem in a VLP system with IRS deployment. An ML estimator utilizing signals from both LOS and IRS components has been presented. Optimal adjustment of IRS orientations that maximizes the received power has

been derived analytically. An algorithm has been proposed to improve positioning accuracy in the absence of LOS signals. A generic CRLB expression has been derived and employed as a benchmark for evaluating the performance of the proposed algorithm. Various simulations have been conducted to verify the analytical results and to investigate the performance of the proposed positioning approach. We have also analyzed the impacts of IRS parameters, namely the fraction of the diffuse component and the directivity, on the positioning accuracy. Finally, the effects of using IRSs in the presence of LOS paths on the positioning accuracy have further been investigated for various positions of the VLC receiver. It has been concluded that although IRSs do no provide critical improvements in positioning accuracy in the presence of LOS signals from a sufficient number of LED transmitters, they can be very important in achieving accurate positioning when all or most of LOS paths are blocked. Therefore, IRS-aided VLP systems can be utilized in various applications such as navigation of robots and tracking of critical devices in various environments (e.g., factory or hospital) with both LOS and NLOS conditions.

In this study, the VLC receiver is assumed to know the parameters of IRSs perfectly. An important extension can be the consideration of imperfect knowledge at the VLC receiver about IRS related parameters, such as orientations and reflection coefficients, and investigation of its effects on position estimation accuracy. Another interesting direction for future work is related to the analysis of the effects of multipath components in the environment on positioning accuracy of IRS-aided VLP systems. Finally, experimental studies can be performed to evaluate the proposed approaches in real positioning applications.

REFERENCES

[1] M. Yoshino, S. Haruyama, and M. Nakagawa, "High-accuracy positioning system using visible LED lights and image sensor," in *2008 IEEE Radio and Wireless Symposium*, 2008, pp. 439–442.

[2] J. Luo, L. Fan, and H. Li, "Indoor positioning systems based on visible light communication: State of the art," *IEEE Communications Surveys & Tutorials*, vol. 19, no. 4, pp. 2871–2893, 4th Quart. 2017.

[3] M. F. Keskin, A. D. Sezer, and S. Gezici, "Localization via visible light systems," *Proceedings of the IEEE*, vol. 106, no. 6, pp. 1063–1088, June 2018.

[4] J. Armstrong, Y. Sekercioglu, and A. Neild, "Visible light positioning: A roadmap for international standardization," *IEEE Communications Magazine*, vol. 51, no. 12, pp. 68–73, Dec. 2013.

[5] H. Steendam, T. Q. Wang, and J. Armstrong, "Cramer-Rao bound for AOA-based VLP with an aperture-based receiver," in *2017 IEEE International Conference on Communications (ICC)*, 2017, pp. 1–6.

[6] M. F. Keskin, S. Gezici, and O. Arikan, "Direct and two-step positioning in visible light systems," *IEEE Transactions on Communications*, vol. 66, no. 1, pp. 239–254, Jan. 2018.

[7] B. Zhou, A. Liu, and V. Lau, "On the fundamental performance limit of visible light-based positioning," in *13th International Conference on Signal Processing and Communication Systems (ICSPCS)*, 2019, pp. 1–6.

[8] M. Yasir, S.-W. Ho, and B. N. Vellambi, "Indoor position tracking using multiple optical receivers," *Journal of Lightwave Technology*, vol. 34, no. 4, pp. 1166–1176, Feb. 2016.

[9] S. Shen, S. Li, and H. Steendam, "Simultaneous position and orientation estimation for visible light systems with multiple LEDs and multiple PDs," *IEEE Journal on Selected Areas in Communications*, vol. 38, no. 8, pp. 1866–1879, 2020.

[10] E. Basar, M. Di Renzo, J. De Rosny, M. Debbah, M.-S. Alouini, and R. Zhang, "Wireless communications through reconfigurable intelligent surfaces," *IEEE Access*, vol. 7, pp. 116 753–116 773, 2019.

[11] Q. Wu and R. Zhang, "Intelligent reflecting surface enhanced wireless network via joint active and passive beamforming," *IEEE Transactions on Wireless Communications*, vol. 18, no. 11, pp. 5394–5409, 2019.

[12] Z. Yang, M. Chen, W. Saad, W. Xu, M. Shikh-Bahaei, H. V. Poor, and S. Cui, "Energy-efficient wireless communications with distributed reconfigurable intelligent surfaces," *IEEE Transactions on Wireless Communications*, vol. 21, no. 1, pp. 665–679, 2022.

[13] A. M. Abdelhady, A. K. S. Salem, O. Amin, B. Shihada, and M.-S. Alouini, "Visible light communications via intelligent reflecting surfaces: Metasurfaces vs mirror arrays," *IEEE Open Journal of the Communications Society*, vol. 2, pp. 1–20, 2021.

[14] S. Sun, T. Wang, F. Yang, J. Song, and Z. Han, "Intelligent reflecting surface-aided visible light communications: Potentials and challenges," *IEEE Vehicular Technology Magazine*, vol. 17, no. 1, pp. 47–56, 2022.

[15] B. Cao, M. Chen, Z. Yang, M. Zhang, J. Zhao, and M. Chen, "Reflecting the light: Energy efficient visible light communication with reconfigurable intelligent surface," in *2020 IEEE 92nd Vehicular Technology Conference (VTC2020-Fall)*, 2020, pp. 1–5.

[16] S. Sun, F. Yang, and J. Song, "Sum rate maximization for intelligent reflecting surface-aided visible light communications," *IEEE Communications Letters*, vol. 25, no. 11, pp. 3619–3623, 2021.

[17] H. Abumarshoud, B. Selim, M. Tatipamula, and H. Haas, "Intelligent reflecting surfaces for enhanced NOMA-based visible light communications," in *IEEE International Conference on Communications (ICC)*, 2022, pp. 571–576.

[18] K. Prabhath, S. K. Jayaweera, and S. A. Lane, "Intelligent reflecting surface orientation optimization to enhance the performance of wireless communications systems," in *2022 International Workshop on Antenna Technology (iWAT)*, 2022, pp. 231–234.

[19] A. R. Ndjiongue, T. M. N. Ngatched, O. A. Dobre, and H. Haas, "Toward the use of re-configurable intelligent surfaces in VLC systems: Beam steering," *IEEE Wireless Communications*, vol. 28, no. 3, pp. 156–162, 2021.

[20] L. Qian, X. Chi, L. Zhao, and A. Chaaban, "Secure visible light communications via intelligent reflecting surfaces," *arXiv:2101.12390*, 2021.

[21] S. Aboagye, A. R. Ndjiongue, T. M. N. Ngatched, O. A. Dobre, and H. V. Poor, "RIS-assisted visible light communication systems: A tutorial," *IEEE Communications Surveys & Tutorials*, vol. 25, no. 1, pp. 251–288, 2023.

[22] A. Nasri, A. H. A. Bafghi, and M. Nasiri-Kenari, "Wireless localization in the presence of intelligent reflecting surface," *IEEE Wireless Communications Letters*, vol. 11, no. 7, pp. 1315–1319, 2022.

[23] M. Ammous and S. Valaee, "Cooperative positioning with the aid of reconfigurable intelligent surfaces and zero access points," in *2022 IEEE 96th Vehicular Technology Conference (VTC2022-Fall)*, 2022, pp. 1–5.

[24] Y. Liu, E. Liu, R. Wang, and Y. Geng, "Reconfigurable intelligent surface aided wireless localization," in *IEEE International Conference on Communications (ICC)*, 2021, pp. 1–6.

[25] N. Afzali, M. J. Omidi, K. Navaie, and N. S. Moayedian, "Low complexity multi-user indoor localization using reconfigurable intelligent surface," in *2022 30th International Conference on Electrical Engineering (ICEE)*, 2022, pp. 731–736.

[26] T. Zhou, K. Xu, Z. Shen, W. Xie, D. Zhang, and J. Xu, "Aoa-based positioning for aerial intelligent reflecting surface-aided wireless communications: An angle-domain approach," *IEEE Wireless Communications Letters*, vol. 11, no. 4, pp. 761–765, 2022.

[27] M. Ammous and S. Valaee, "Positioning and tracking using reconfigurable intelligent surfaces and extended Kalman filter," in *IEEE 95th Vehicular Technology Conference (VTC 2022-Spring)*, 2022, pp. 1–6.

[28] T. Ma, Y. Xiao, X. Lei, W. Xiong, and M. Xiao, "Distributed reconfigurable intelligent surfaces assisted indoor positioning," *IEEE Transactions on Wireless Communications*, vol. 22, no. 1, pp. 47–58, 2023.

[29] A. Elzanaty, A. Guerra, F. Guidi, and M.-S. Alouini, "Reconfigurable intelligent surfaces for localization: Position and orientation error bounds," *IEEE Transactions on Signal Processing*, vol. 69, pp. 5386–5402, 2021.

[30] Z. Wang, Z. Liu, Y. Shen, A. Conti, and M. Z. Win, "Wideband localization with reconfigurable intelligent surfaces," in *2022 IEEE 95th Vehicular Technology Conference (VTC2022-Spring)*, 2022, pp. 1–6.

[31] M. F. Keskin, A. D. Sezer, and S. Gezici, "Optimal and robust power allocation for visible light positioning systems under illumination constraints," *IEEE Transactions on Communications*, vol. 67, no. 1, pp. 527–542, 2019.

[32] A. M. Abdelhady, O. Amin, A. K. S. Salem, and M.-S. Alouini, and B. Shihada, "Channel characterization of IRS-based visible light communication systems," *IEEE Transactions on Communications*, vol. 70, no. 3, pp. 1913–1926, 2022.

[33] S. D. Lausnay, L. D. Strycker, J. P. Goemaere, B. Nauwelaers, and N. Stevens, "A survey on multiple access visible light positioning," in *IEEE International Conference on Emerging Technologies and Innovative Business Practices for the Transformation of Societies (EmergiTech)*, Aug. 2016, pp. 38–42.

[34] D. Karunatilaka, F. Zafar, V. Kalavally, and R. Parthiban, "LED based indoor visible light communications: State of the art," *IEEE Communications Surveys & Tutorials*, vol. 17, no. 3, pp. 1649–1678, 2015.

[35] T. Komine and M. Nakagawa, "Fundamental analysis for visible-light communication system using LED lights," *IEEE Transactions on Consumer Electronics*, vol. 50, no. 1, pp. 100–107, Feb. 2004.

[36] E. Gonendik and S. Gezici, "Fundamental limits on RSS based range estimation in visible light positioning systems," *IEEE Communications Letters*, vol. 19, no. 12, pp. 2138–2141, 2015.

[37] X. Zhang, J. Duan, Y. Fu, and A. Shi, "Theoretical accuracy analysis of indoor visible light communication positioning system based on received signal strength indicator," *Journal of Lightwave Technology*, vol. 32, no. 21, pp. 3578–3584, 2014.

[38] M. F. Keskin and S. Gezici, "Comparative theoretical analysis of distance estimation in visible light positioning systems," *Journal of Lightwave Technology*, vol. 34, no. 3, pp. 854–865, 2016.

[39] J. M. Kahn and J. R. Barry, "Wireless infrared communications," *Proceedings of the IEEE*, vol. 85, no. 2, pp. 265–298, Feb. 1997.

[40] O. Gonzalez, S. Rodriguez, R. Perez-Jimenez, B. Mendoza, and A. Ayala, "Error analysis of the simulated impulse response on indoor wireless optical channels using a Monte Carlo-based ray-tracing algorithm," *IEEE Transactions on Communications*, vol. 53, no. 1, pp. 124–130, 2005.

[41] H. V. Poor, *An Introduction to Signal Detection and Estimation*, 2nd ed. New York: Springer-Verlag, 1994.